DFT and ab initio direct dynamics study on the reaction of H 2 loss reaction from H 2BNH 2

ARTICLE *in* JOURNAL OF MOLECULAR STRUCTURE THEOCHEM · MARCH 2005

Impact Factor: 1.37 · DOI: 10.1016/j.theochem.2004.12.012

3 AUTHORS, INCLUDING:

Jian-Guo Zhang
Beijing Institute of Technology
312 PUBLICATIONS **1,577** CITATIONS

SEE PROFILE

ELSEVIER

Journal of Molecular Structure: THEOCHEM 717 (2005) 33–39

THEO CHEM

www.elsevier.com/locate/theochem

DFT and ab initio direct dynamics study on the reaction of H_2 loss reaction from H_2BNH_2

Jianguo Zhang, Shaowen Zhang, Qian Shu Li*

The State Key Laboratory of Prevention and Control of Explosion Disasters, School of Science, Beijing Institute of Technology, Beijing 100081, People's Republic of China

Received 16 November 2004; revised 1 December 2004; accepted 1 December 2004
Available online 11 January 2005

Abstract

DFT and ab initio molecular orbital calculations are carried out for the H_2 loss reaction from aminoborane (H_2BNH_2). The geometries of all the stationary points are optimized at the B3LYP and MP2 methods with a series of basis sets up to aug-cc-pVTZ. The harmonic vibrational frequencies are calculated at the same level of theory. One transition state is found at the B3LYP/(aug-)cc-pVTZ and MP2/(aug-)cc-pVTZ level of theory. The energies and enthalpies are refined at the G3, G3MP2, G3MP2B3, CBS-Q, CBS-QB3, and HL methods based on the geometries optimized using B3LYP/aug-cc-pVTZ method. The rate constants are evaluated using the conventional transition-state theory (TST), canonical variational transition-state theory (CVT), and canonical variational transition-state theory with small curvature tunneling correction (CVT/SCT) and conventional transition-state theory with Eckart tunneling correction (TST/Eckart).

Keywords: Aminoborane; Iminoborane; Unimolecular decomposition; Ab initio calculation; Vibrational transition state theory; Rate constant

1. Introduction

Aminoborane, H_2BNH_2, the B–N analogue of ethylene was first detected in a mass spectrometric study [1] and formed in the thermal decomposition of H_3BNH_3 [2,3]. It has received extensive experimental [4–8] and theoretical attentions [9–13] due to its importance as a basic unit for complex aminoborane. Carpenter presented the infrared matrix isolation characterization of aminoborane [8]. Ha [9] calculated the equilibrium geometries, rotational constants and vibrational frequencies of aminoborane, diaminoborane and aminodifluoroborane with ab initio SCF method and he found that the appreciable amount of the double bond character existed these molecules. Then, Mo [12] and Minyaev [13] reported the reaction paths and the theoretical analysis for the internal rotation in aminoborane. Gerry [14] measured its high-resolution infrared spectrum. Briggs [15] determined the microwave spectrum, the molecular structure and the quadrupole coupling constants of H_2BNH_2. Komm [16] reported the preparation and characterization about poly(aminoborane). Recently, Suresh [17] studied the conjugation involving nitrogen lone-pair electrons of some boron–nitrogen compounds.

It has been shown that H_3BNH_3 can be a potential chemical hydrogen (H_2) storage medium for fuel cell and other applications [18] since its moderate decomposition temperatures, the exothermic character of the decomposition process and the relatively high hydrogen content. Recently, the H_2 release process of the H_3BNH_3 has been concerned by many experimental [3,18–22] studies. In 1985, Geanangel and Wendlandt [20] described the process of three stepwise hydrogen loss from H_3BNH_3 to BN by thermogravimetry (TG) and differential scanning calorimetry (DSC) technologies. And then, they suggested the thermal dissociation of H_3BNH_3 by differential thermal analysis (DTA) curves and better defined the chemical steps in

* Corresponding author. Tel./fax: +86 10 68912665.
E-mail address: qsli@bit.edu.cn (Q.S. Li).

0166-1280/$ - see front matter © 2004 Elsevier B.V. All rights reserved.
doi:10.1016/j.theochem.2004.12.012

the decomposition reaction of H_3BNH_3 [3]. Carpenter and Ault studied the pyrolysis of the adduct H_3BNH_3 and observed the evidence of H_2BNH_2 [23]. Quite recently, the thermally activated decomposition of ammonia–borane has been investigated by using combined thermoanalytical methods by Baitalow et al. [18,19], which indicated that H_3BNH_3 underwent stepwise thermal decomposition in the temperature range up to 500 K and the decomposition reaction is accompanied by hydrogen evolution. Wolf assumed that the monomeric aminoborane might be a reactive intermediate during the formation of borazine at the thermal decomposition of H_3BNH_3 [18,19]. Eventually borazine is formed from H_2BNH_2 via a dehydrogenation to the highly reactive monomeric iminoborane HBNH [24] and the trimerization of HBNH.

Thus it can be seen that the reaction of H_2 loss from H_2BNH_2 is an important step during the decomposition of H_3BNH_3. In order to provide detailed dynamics information on the reaction and obtain the rate constants over a wide temperature range of the hydrogen elimination from the H_2BNH_2, high-level ab initio calculation and rate constants calculation are still required. The aim of the present work is to perform a theoretical calculation on the reaction of $H_2BNH_2 \rightarrow HBNH + H_2$ to provide reliable results for the reaction enthalpy, reaction potential energy surface (PES) and the gas phase rate constant.

2. Methodology

2.1. Electronic structure calculations

The geometries and frequencies of all stationary points (reactants, products, and the transition state) are optimized at the B3LYP [25] and MP2 [26–28] methods of theory with (aug-)cc-pVDZ [29–31] and (aug-)cc-pVTZ basis sets [29]. To yield more reliable reaction enthalpy and barrier, the higher-level energies calculations for all stationary points are further performed with the G3 [32], G3MP2 [33], G3MP2B3 [34], CBS-Q [35], CBS-QB3 [36,37], and a combination method [38,39] (denoted as HL) based on the optimized geometries at the B3LYP/aug-cc-pVTZ levels of theory. Here, the method employ a combination of quadratic configuration interaction calculations with perturbative inclusion of the triplet contribution, QCISD(T) [40], and second-order Møller–Plesset perturbation theory (MP2) [26–28]. And he estimate the infinite basis set limit via the extrapolation of results obtained for sequences of the correlation-consistent polarized-valence basis sets. The higher-level estimate, E_{HL} is obtained as the sum of the QCISD(T) extrapolations. The combination of extrapolations can be expressed as [38]:

$$E_{HL} = E[\mathrm{QCISD}(T)/\mathrm{cc-pVTZ}] + \{E[\mathrm{QCISD}(T)/\mathrm{cc-pVTZ}] - E[\mathrm{QCISD}(T)/\mathrm{cc-pVDZ}]\} \times 0.46286 + E[\mathrm{MP2/cc-pVQZ}]$$

$$+\{E[\mathrm{MP2/cc-pVQZ}] - E[\mathrm{MP2/cc-pVTZ}]\} \times 0.69377 + E[\mathrm{MP2/cc-pVTZ}] + \{E[\mathrm{MP2/cc-pVTZ}] - E[\mathrm{MP2/cc-pVDZ}]\} \times 0.46286$$

In order to reduce computation cost, the minimum energy path (MEP) is obtained using the intrinsic reaction coordinate (IRC) method [41] at the B3LYP/aug-cc-pVTZ levels of theory. In the calculation of rate

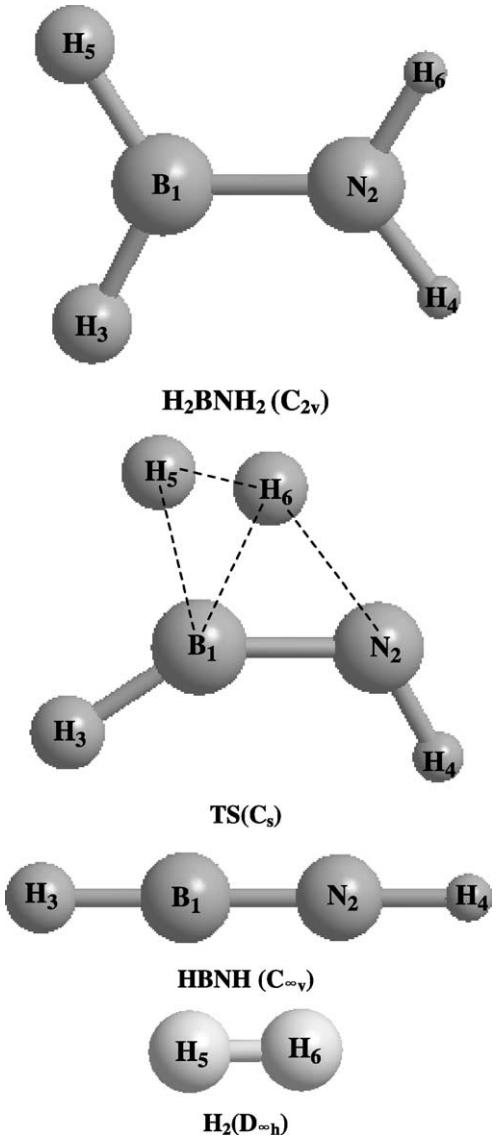

Fig. 1. Pictorial of optimized geometries of the stationary points.

constants, the single point energies of MEP are obtained from the Miller's method [38] based on the optimized geometries at the B3LYP/aug-cc-pVTZ levels of theory. All the electronic structure calculations are carried out using the GAUSSIAN 03 program [42].

2.2. The rate constant calculations

The rate constants are calculated using the conventional transition-state theory (TST), canonical variational transition-state theory [43,44] (CVT), canonical variational transition-state theory with small curvature tunneling correction [45] (CVT/SCT) and the conventional transition-state theory rate constant calculations with the Eckart tunneling correction (TST/Eckart) [46] by employing the online Vklab program package [47] and Polyrate 8.2 program [48].

In the present study, the reaction coordinate, s is defined as the distance along the MEP with the origin located at the saddle point and is negative on the reactant side and positive on the product side. For canonical ensemble at a given temperature T, the canonical variational theory (CVT) thermal rate constant is given by

$$k^{\mathrm{CVT}}(T) = \min_{s} k^{\mathrm{GT}}(T,s)$$

with

$$k^{\mathrm{GT}}(T,s) = \left\{ \sigma \frac{k_{\mathrm{B}}T}{h} \frac{Q^{\mathrm{GT}}(T,s)}{\Phi^{\mathrm{R}}(T)} \mathrm{e}^{-V_{\mathrm{MEP}}(s)/k_{\mathrm{B}}T} \right\}$$

where $k^{\mathrm{GT}}(T,s)$ is the generalized transition state theory rate constant at the dividing surface which intersects the MEP at s and is orthogonal to the MEP at the intersection point. σ is the symmetry factor accounting for the possibility of more than one symmetry related reaction path and can be calculated as the ratio of the product of the reactant rotational symmetry numbers to that of the transition state. k_{B} is Boltzman's constant and h is Plank's constant. Q^{GT} is the internal partition function of the generalized transition state with the local zero of energy at $V_{\mathrm{MEP}}(s)$, which is the classical potential energy along the minimum energy path s with its zero of energy at the reactants. Φ^{R} is the reactant partition function per unit volume for bimolecular reactions. Both the Q^{GT} and Φ^{R} are

Table 1
The optimized geometries of reactants, products and transition states using the several methods with different basis set

Species	Parameters[a]	B3LYP/D	B3/AD	B3/T	B3/AT	MP2/D	MP2/AD	MP2/T	MP2/AT	Exp.
H_2BNH_2	R(1,2)	1.389	1.388	1.393	1.390	1.396	1.404	1.392	1.395	1.391[b]
(C_{2v})	R(1,3)	1.192	1.192	1.202	1.206	1.207	1.204	1.190	1.191	1.195[b]
	R(2,5)	1.006	1.006	1.011	1.014	1.023	1.012	1.004	1.005	1.004[b]
	A(2,1,3)	119.0	119.0	119.0	119.0	118.9	118.7	118.8	118.8	
	A(3,1,4)	121.9	122.0	122.1	122.0	122.2	122.6	122.4	122.5	122.2[b]
	A(1,2,5)	123.3	123.3	123.3	123.3	123.1	123.0	123.1	123.1	
	A(5,2,6)	113.3	113.4	113.5	113.3	113.8	113.9	113.8	113.7	114.2[b]
TS (C_s)	R(1,2)	1.357	1.359	1.352	1.352	1.376	1.379	1.365	1.367	
	R(1,3)	1.200	1.196	1.188	1.188	1.201	1.199	1.186	1.187	
	R(1,5)	1.378	1.366	1.354	1.354	1.363	1.360	1.345	1.346	
	R(1,6)	1.351	1.345	1.332	1.333	1.347	1.352	1.332	1.336	
	R(2,4)	1.025	1.021	1.015	1.014	1.027	1.024	1.014	1.014	
	R(2,6)	1.462	1.459	1.444	1.445	1.455	1.446	1.434	1.432	
	R(5,6)	0.998	0.998	0.987	0.986	0.985	0.986	0.971	0.973	
	A(2,1,3)	144.8	144.2	144.2	144.2	144.6	144.8	144.6	144.7	
	A(2,1,5)	103.6	104.0	104.2	104.2	102.8	102.9	103.3	103.3	
	A(2,1,6)	65.4	65.4	65.2	65.1	64.6	64.0	64.2	64.0	
	A(3,1,5)	110.6	110.9	110.7	110.8	111.4	111.3	111.1	111.2	
	A(3,1,6)	140.8	141.8	142.5	142.9	141.1	143.3	143.4	144.1	
	A(5,1,6)	42.9	43.2	43.1	43.1	42.6	42.6	42.5	42.5	
	A(1,2,4)	118.4	119.1	120.5	120.9	116.7	119.1	119.7	120.4	
	D(3,1,2,4)	0.5	2.0	1.8	−2.3	−1.0	1.4	0.7	1.4	
	D(5,1,2,4)	−165.6	−165.2	−165.3	165.2	−165.5	−165.4	−165.9	−165.9	
	D(6,1,2,4)	−145.6	−145.5	−145.6	146.8	−145.9	−147.5	−148.7	−149.1	
HBNH	R(1,2)	R(1,2)	1.241	1.239	1.234	1.234	1.253	1.255	1.244	1.238[c]
($C_{\infty v}$)	R(2,4)	R(2,4)	0.998	0.998	0.991	0.992	1.000	1.001	0.991	
	R(1,3)	R(1,3)	1.177	1.172	1.166	1.166	1.180	1.177	1.166	
H_2 ($D_{\infty h}$)	R(5,6)	0.7617	0.7608	0.7429	0.7429	0.7541	0.7549	0.7372	0.7372	0.741[d]

About the basis sets: cc-pVDZ, aug-cc-pVDZ, cc-pVTZ and aug-cc-pVTZ is abbreviated by D, AD, T and AT.

[a] Bond lengths in Å and bond angles in deg.

[b] Ref. [53].

[c] Ref. [52].

[d] Ref. [56].

approximated as products of electronic, rotational, and vibrational partition functions. For Φ^{R}, the relative translational partition function is also included. Translational and rotational partition functions are evaluated classically, whereas, the vibrational partition functions are calculated quantum mechanically within the harmonic approximation for the present studies.

Furthermore, the CVT rate constants are corrected with the small-curvature tunneling (SCT) [49–51] transmission coefficient. The SCT transmission coefficients, that include the reaction-path curvature effect on the transmission probability, are based on the centrifugal-dominant small curvature semi-classical adiabatic ground-state (CD-SCSAG) approximation. In particular, the transmission probability at energy E is given by

$$P(E) = \frac{1}{\{1 + e^{-2\theta(E)}\}}$$

where $\theta(E)$ is the imaginary action integral evaluated along the reaction coordinate

$$\theta(E) = \frac{2\pi}{h} \int_{s_l}^{s_r} \sqrt{2\mu_{eff}(s)|E - V_a^G(s)|}ds$$

and where the integration limits s_l and s_r are the reaction coordinate classical turning points. The reaction-path curvature effect on the tunneling probability is included in the effective reduced mass μ_{eff}.

3. Results and discussion

3.1. Stationary points

The optimized structures for the stationary points obtained at the B3LYP/aug-cc-pVTZ levels of theory are given in Fig. 1. Table 1 lists the optimized geometric parameters of the equilibrium and transition states structures of the reaction at the B3LYP and MP2 methods with (aug-)cc-pVDZ and (aug-)cc-pVTZ basis sets along with the available experimental data. The optimized geometrical parameters of H_2BNH_2, HBNH, and H_2 at all the levels of theory employed are in good agreement with the available experimental values [52,53]. For the transition state, the predicted geometries also agree with each other between all the levels of theory. Compared the results, we can find that the structure is

Table 2
Harmonic frequencies (cm^{-1}), the code and integers in parentheses are the symmetry and infrared intensities (km/mol) and zero point energies (kcal mol^{-1}) for the reactants, products and transition states using several methods with the difference basis set

Species	Methods	Harmonic frequencies (cm^{-1}) and infrared intensities (km/mol)	ZPE
H_2BNH_2 (C_{2v})	B3LYP/cc-pVTZ	620(b1,179), 749(b2,0), 857(a2,0), 1015(b1,27), 1139(b2,34), 1159(a1,1), 1363(a1,54), 1647(a1,70), 2577(a1,92), 2651(b2,164), 3585(a1,19), 3675(b2,24)	30.08
	B3LYP/aug-cc-pVTZ	622(b1,173), 748(b2,0), 852(a2,0), 1017(b1,26), 1137(b2,34), 1156(a1,1), 1357(a1,65), 1648(a1,74), 2578(a1,97), 2653(b2,165), 3583(a1,19), 3670(b2,26)	30.05
	MP2/cc-pVTZ	615(b1,185), 744(b2,0), 872(a2,0), 1029(b1,27), 1147(b2,36), 1174(a1,1), 1379(a1,57), 1647(a1,73), 2626(a1,95), 2710(b2,165), 3635(a1,38), 3747(b2,36)	30.49
	MP2/aug-cc-pVTZ	609(b1,177), 739(b2,0), 864(a2,0), 1030(b1,26), 1140(b2,35), 1167(a1,1), 1368(a1,70), 1649(a1,77), 2624(a1,99), 2708(b2,163), 3623(a1,34), 3732(b2,37)	30.38
	Exptl.[a]	670, 593, 763, 1005, 1131, 1225, 1337, 1625, 2495, 2564, 3451, 3534	
TS (C_s)[b]	B3LYP/cc-pVTZ	−1522(586), 419(52), 868(41), 927(64), 996(39), 1045(108), 1266(42), 1450(97), 2119(241), 2172(45), 2658(100), 3525(11)	25.01
	B3LYP/aug-cc-pVTZ	−1523(608), 412(48), 865(42), 920(60), 992(40), 1040(102), 1264(41), 1494(110), 2116(237), 2167(42), 2659(100), 3522(8)	24.95
	MP2/cc-pVTZ	−1492(652), 430(69), 867(47), 925(58), 1027(23), 1053(95), 1313(46), 1488(75), 2219(180), 2235(109), 2718(90), 3570(17)	25.51
	MP2/aug-cc-pVTZ	−1496(688), 408(64), 862(48), 910(54), 1019(24), 1043(88), 1308(47), 1479(88), 2207(142), 2229(138), 2711(90), 3565(19)	25.36
HBNH ($C_{\infty v}$)	B3LYP/cc-pVTZ	469×2(π,121), 742×2(π,1), 1844(σ,45), 2855(σ,12), 3878(σ,197)	15.77
	B3LYP/aug-cc-pVTZ	472×2(π,117), 751×2(π,1), 1839(σ,59), 2889(σ,15), 3864(σ,197)	15.78
	MP2/cc-pVTZ	480×2(π,111), 727×2(π,2), 1799(σ,20), 2914(σ,9), 3875(σ,196)	15.75
	MP2/aug-cc-pVTZ	477×2(π,106), 738×2(π,2), 1789(σ,31), 2912(σ,6), 3891(σ,205)	15.74
	Eeptl.[c]	462, 464, 678, 683, 1819, 2796, 3712	
H_2 ($D_{\infty h}$)	B3LYP/cc-pVTZ	4419(sgg,0)	6.32
	B3LYP/aug-cc-pVTZ	4418(sgg,0)	6.32
	MP2/cc-pVTZ	4524(sgg,0)	6.47
	MP2/aug-cc-pVTZ	4522(sgg,0)	6.46
	Exptl.[d]	4355	

[a] Ref. [53].
[b] There is only a image frequency (showed in the table in bold, italic and underline style) for TS.
[c] Ref. [55].
[d] Ref. [57].

Table 3
The reaction energetic parameters (kcal/mol) at different levels of theory

Method	ΔE	$V^{\neq}$	$V_a^{G\neq}$	$\Delta H^{\circ}_{298\ K}$	$\Delta G^{\circ}_{298\ K}$
B3LYP/cc-pVDZ	39.50	77.23	72.26	33.49	25.44
B3LYP/aug-cc-pVDZ	39.59	76.98	71.96	33.58	25.57
B3LYP/cc-pVTZ	37.80	77.95	72.88	31.76	23.77
B3LYP/aug-cc-pVTZ	37.72	77.72	72.62	31.72	23.74
MP2/cc-pVDZ	36.56	78.08	73.26	30.21	22.16
MP2/aug-cc-pVDZ	37.00	77.03	72.06	30.74	22.70
MP2/cc-pVTZ	36.98	77.75	72.77	30.67	22.69
MP2/aug-cc-pVTZ	36.89	77.17	72.15	30.66	22.69
MP2/cc-pVQZ// B3LYP/aug-cc-pVTZ	36.71	77.45	72.34	30.71	22.72
E_{HL}//B3LYP/aug-cc-pVTZ	37.49	78.11	73.00	31.48	23.50
G3			74.74	29.36	23.35
G3MP2			74.01	27.97	21.96
G3MP2B3			73.93	27.66	21.66
CBS-Q			74.44	28.62	22.61
CBS-QB3			73.98	28.53	22.53

good approximation between B3LYP/cc-pVTZ and MP2/cc-pVTZ method of theory, and that the structures is very close using the same method from different basis set. In particular, we can nearly obtain the same structure at the B3LYP/cc-pVTZ and B3LYP (MP2)/aug-cc-pVTZ level of theory. So, we can say that the diffuse function for the calculation is unnecessary.

Table 2 abstracts the harmonic vibrational frequencies, their infrared intensities and zero point energies of the equilibrium and transition states structure of the reaction at the B3LYP and MP2 levels of theory with the difference basis set along with the previous calculated results [54] and the available experimental data [24,52,53,55]. The largest relative deviation between theoretical prediction and experimental measurements is only 10%. In particular, MP2/cc-pVTZ and B3LYP/cc-pVTZ provide good prediction of frequencies for all modes. Even if for the imaginary frequency of the transition state, the theoretical predictions are quite consistent with each other among the results from different methods. The predicted values of the imaginary frequency are 1522*i*, 1523*i*, 1492*i*, and 1496*i* cm^{-1} at the B3LYP/cc-pVTZ, B3LYP/aug-cc-pVTZ, MP2/cc-pVTZ, and MP2/aug-cc-pVTZ, levels of theory, respectively. So, we can know that the shapes of MEP near the transition state among different methods are very similar. In this paper, we employ the results for the TS and IRC calculations from B3LYP/aug-cc-pVTZ method of theory.

Table 3 lists the reaction energies (ΔE), the classical potential barriers ($V^{\neq}$), the vibrational adiabatic ground-state potential ($V_a^{G\neq}$), the theoretical reaction enthalpies ($\Delta H^{\circ}_{298\ K}$) and the reaction free energies. The predicted values of these properties are quite consistent at the same method with different basis sets, however are quite scattered among different methods. When we refine these energies using different methods based on the B3LYP/aug-cc-pVTZ geometry, the values of each property are very close.

3.2. Reaction path properties

Fig. 2 shows the variation of bond-lengths along IRC at B3LYP/aug-cc-pVTZ levels of theory. Along with the increasing of the breaking bond lengths of B_1–H_5 and N_2–H_6 and the decreasing of the bond distances of the H_5–H_6, the H_5–H_6 new bond are formed and the hydrogen molecule loss from H_2BNH_2 are completed. The B_1–H_3 and N_2–H_4 bonds remain unchanged in the course of the reaction. The bond length of the broking bond N_2–H_6 changes more sharply than that of the breaking bond B_1–H_5 during the reaction process, so the forming H_5–H_6 to the B atom is closer than to nitrogen atom in the translated state structure. And the B_1–N_2 bond is changed from 1.390 Å (in aminoborane, H_2BNH_2) to 1.234 Å (iminoborane, HBNH), so it becomes shorter and shorter from reactant to product.

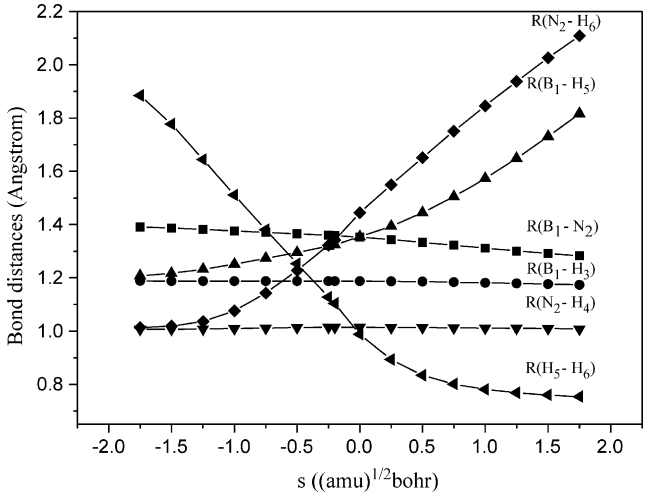

Fig. 2. The changes of bond distances as functions of *s* $(amu)^{1/2}$ bohr at the B3LYP/aug-cc-pVTZ level of theory.

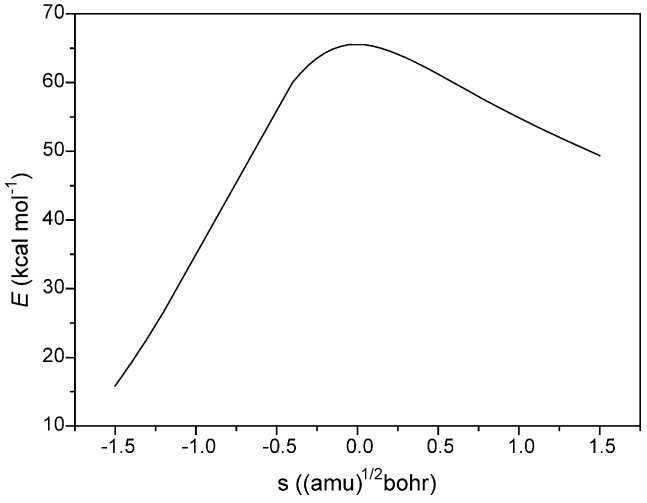

Fig. 3. The vibrationally adiabatic ground-state potential energy curves (V_a^G) if the reaction as a function of s (amu)$^{1/2}$ bohr at the B3LYP/aug-cc-pVTZ level of theory.

Fig. 3 depicts the vibrtionally adiabatic ground-state potential energy curves (V_a^G) of the reaction as a function of s (amu)$^{1/2}$ bohr using the fine energies from Miller's method based on B3LYP/aug-cc-pVTZ level of theory using the interpolated method. It can be seen that for the reaction the V_a^G curve at the method is an ideal potential surface.

3.3. Rate constant calculations

We calculate the rate constants using CVT, CVT/ZCT, CVT/SCT, TST, and TST/Eckart methods based on the interpolated MEP by the fine energies from the higher-level method [38] based on the optimized geometries at the B3LYP/aug-cc-pVTZ levels of theory. The rate constants are showed in Fig. 4. At 200 K, the rate constant of TST/Eckart is the largest among all methods. However, the rate constants of TST, CVT, CVT/SCT and CVT/ZCT become almost identical as temperature higher than 1000 K. The rate constant of TST/Eckart is higher than CVT/SCT and those of CVT/ZCT, and the rate constant of CVT is very similar to those of TST in the whole temperature range. It is obvious that the vibrational effect and tunneling effect are important at low temperature, so the rate for the H_2 loss from H_2BNH_2 is sizeable, which is according with the experimental results [18]. The fitted Arrhenius expression calculated from CVT/SCT method using the interpolated B3LYP/aug-cc-pVTZ MEP is $k(T) = 1.58 \times 10^9 \times T^{1.20} \times e^{(-3.49\times10^4/T)}$ s^{-1}. At the other side, these kinetics data need to be verified by new experimental results.

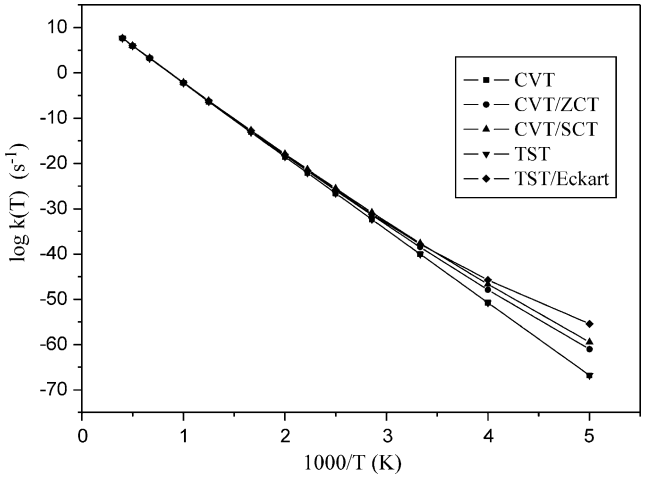

Fig. 4. Arrhenius plots of the rate constants calculated at CVT, CVT/ZCT, CVT/SCT, TST and TST/Eckart levels of theory. The rate constants are calculated based on the interpolated MEP at the B3LYP/aug-cc-pVTZ level of theory.

4. Summary

In the present study, a direct dynamics study of thermal rate constants of the H_2 loss reaction from ammonia borane (H_2BNH_2) has been carried out employing B3LYP and ab initio calculations. The geometries, harmonic vibrational frequencies of all the stationary points are calculated by means of B3LYP and MP2 levels of theory with both (aug-)cc-pVDZ and (aug-)cc-pVTZ basis sets. The potential energy surface information is carried out at B3LYP/aug-cc-pVTZ level of theory. The energies and enthalpies are refined at the G3, G3MP2, G3MP2B3, CBS-Q, CBS-QB3, and Miller's method based on the geometries optimized using B3LYP/aug-cc-pVTZ method. The energies of the single points along the minimum energy path are obtained using interpolated method. The rate constants of the reaction are calculated by TST, CVT, CVT/SCT, CVT/ZCT, and TST/Eckart methods.

Acknowledgements

Our thanks are due to D.G. Truhlar for providing the POLYRATE 8.2 program. This work is supported by the National Natural Science Foundation of China (Nos. 20373007 and 20471008) and the Foundation for basic research by the Beijing Institute of Technology.

References

[1] B.W. Boddeker, S.G. Shore, R.K. Bunting, J. Am. Chem. Soc. 88 (1966) 4396.
[2] P.M. Kuznesof, D.F. Shriver, F.E. Stafford, J. Am. Chem. Soc. 90 (1968) 2557.
[3] V. Sit, R.A. Geanangel, W.W. Wendlandt, Thermochim. Acta 113 (1987) 379.
[4] K.G. Hancock, Y. Ko, D.A. Dickinson, J.D. Kramer, J. Organomet. Chem. 90 (1975) 23.
[5] J.M. Sugie, H. Takeo, C. Matsumure, Chem. Phys. Lett. 64 (1979) 573.

[6] M. Sugie, H. Takeo, C. Matsumure, J. Mol. Spectrosc. 123 (1987) 286.
[7] N.P.C. Westwood, N.H. Werstiuk, J. Am. Chem. Soc. 108 (1986) 891.
[8] J.D. Carpenter, B.S. Ault, J. Phys. Chem. 95 (1991) 3502.
[9] T.K. Ha, J. Mol. Struct. (Theochem) 136 (1986) 165.
[10] M.L. McKee, Inorg. Chem. 38 (1999) 321.
[11] J.V. Ortiz, Chem. Phys. Lett. 156 (1989) 489.
[12] Y. Mo, S.D. Peyerimhoff, Theor. Chem. Acc. 101 (1999) 311.
[13] R.M. Minyaev, D.J. Wales, T.R. Walsh, J. Phys. Chem. A 101 (1997) 1384.
[14] M.C.L. Gerry, W. Lewis-Bevan, A.J. Merer, N.P.C. Westwood, J. Mol. Spectrosc. 110 (1985) 153.
[15] T.S. Briggs, W.D. Gwinn, W.L. Jolly, L.R. Thorne, J. Am. Chem. Soc. 100 (1978) 7762.
[16] R. Komm, R.A. Geanangel, R. Liepins, Inorg. Chem. 22 (1983) 1684.
[17] C.H. Suresh, N. Koga, Inorg. Chem. 39 (2000) 3718.
[18] F. Baitalow, J. Baumann, G. Wolf, K. Jaenicke-Rlobler, G. Leitner, Thermochim. Acta 391 (2002) 159.
[19] G. Wolf, J. Baumann, F. Baitalow, F.P. Hoffmann, Thermochim. Acta 343 (2000) 19.
[20] R.A. Geanangel, W.W. Wendlandt, Thermochim. Acta 86 (1985) 375.
[21] J.S. Wang, R.A. Geanangel, Inorg. Chim. Acta 148 (1988) 185.
[22] G. Wolf, J.C. van Miltenburg, U. Wolf, Thermochim. Acta 317 (1998) 111.
[23] J.D. Carpenter, B.S. Ault, Chem. Phys. Lett. 197 (1992) 171.
[24] E.R. Lory, R.F. Porter, J. Am. Chem. Soc. 95 (1973) 1766.
[25] A.D. Becke, J. Chem. Phys. 104 (1996) 1040.
[26] M.J. Frisch, M. Head-Gordon, J.A. Pople, Chem. Phys. Lett. 166 (1990) 275.
[27] M.J. Frisch, M. Head-Gordon, J.A. Pople, Chem. Phys. Lett. 166 (1990) 281.
[28] M. Head-Gordon, J.A. Pople, M.J. Frisch, Chem. Phys. Lett. 153 (1988) 503.
[29] T.H. Dunning Jr., J. Chem. Phys. 90 (1989) 1007.
[30] R.A. Kendall, T.H. Dunning Jr., R.J. Harrison, J. Chem. Phys. 96 (1992) 6796.
[31] D.E. Woon, T.H. Dunning Jr., J. Chem. Phys. 98 (1993) 1358.
[32] L.A. Curtiss, K. Raghavachari, P.C. Redfern, V. Rassolov, J.A. Pople, J. Chem. Phys. 109 (1998) 7764.
[33] L.A. Curtiss, P.C. Redfern, K. Raghavachari, V. Rassolov, J.A. Pople, J. Chem. Phys. 110 (1999) 4703.
[34] A.G. Baboul, L.A. Curtiss, P.C. Redfern, K. Raghavachari, J. Chem. Phys. 110 (1999) 7650.
[35] J.W. Ochterski, G.A. Petersson, J.A. Montgomery Jr., J. Chem. Phys. 104 (1996) 2598.
[36] J.A. Montgomery Jr., M.J. Frisch, J.W. Ochterski, G.A. Petersson, J. Chem. Phys. 110 (1999) 2822.
[37] J.A. Montgomery Jr., M.J. Frisch, J.W. Ochterski, G.A. Petersson, J. Chem. Phys. 112 (2000) 6532.
[38] J.A. Miller, S.J. Klippenstein, J. Phys. Chem. A 107 (2003) 2680.
[39] J.M.L. Martin, Chem. Phys. Lett. 256 (1996) 669.
[40] J.A. Pople, M. Head-Gordon, K. Raghavachari, J. Chem. Phys. 87 (1987) 5968.
[41] C. Gonzalez, H.B. Schlegel, J. Chem. Phys. 90 (1989) 2154.
[42] M.J. Frisch, G.W. Trucks, H.B. Schlegel, G.E. Scuseria, M.A. Robb, J.R. Cheeseman, V.G. Zakrzewski, J.A. Montgomery, R.E. Stratmann, J.C. Burant, S. Dapprich, A.D. Daniels, K.N. Kudin, M.C. Strain, O. Farkas, J. Tomasi, V. Barone, M. Cossi, R. Cammi, B. Mennucci, C. Pomelli, C. Adamo, S. Clifford, J. Ochterski, G.A. Peterson, P.Y. Ayala, Q. Cui, K. Morokuma, D.K. Malik, A.d. Rabuk, K. Raghavachari, J.B. Foresman, J. Cioslowski, J.V. Ortiz, B.B. Stefanov, G. Liu, A. Liashenko, P. Piskorz, I. Komaromi, R. Gomperts, R.L. Martin, D.J. Fox, T. Keith, M.A. Al-Laham, C.Y. Peng, A. Nanayakkara, C. Gonzalez, M. Chalacombe, P.M.W. Gill, B.G. Johnson, W. Chen, M.W. Wong, J.L. Andres, M. Head-Gordon, E.S. Replogle, J.A. Pople, GAUSSIAN 98. Gaussian Inc., Pittsburgh, PA, 1998.
[43] D.G. Truhlar, P.L. Fast, J. Chem. Phys. 109 (1998) 3721.
[44] N.T. Truong, J. Chem. Phys. 100 (1994) 8014.
[45] D.G. Truhlar, A.D. Isaacson, R.T. Skodje, B.C. Garrett, J. Phys. Chem. 86 (1982) 2252.
[46] T. Baer, W.L. Hase, Unimolecular Reaction Dynamics (International Series of Monographs on Chemistry), Oxford University Press, New York, 1996.
[47] S.-W. Zhang, T.N. Truong, VKLab version 1.0, University of Utah, 2001.
[48] Y.Y. Chuang, J.C. Corchado, P.L. Fast, J. Vill, W.-P. Hu, Y.-P. Liu, G.C. Lynch, C.F. Jackels, K.A. Nguyen, M.Z. Gu, I. Rossi, E.L. Isaacson, D.G. Truhlar, Polyrate, Program vision 8.2, Minneapolis, 1999.
[49] D.G. Truhlar, A.D. Isaacson, B.C. Garrett,, CRC, Boca Raton, FL, 1985.
[50] R. Steckler, W.-P. Hu, Y.-P. Liu, G.C. Lynch, B.C. Garret, A.D. Isaacson, V.S. Melissas, D.-H. Lu, T.N. Troung, S.N. Rai, G.C. Hancock, J.G. Lauderdale, T. Joseph, D.G. Truhlar, Comput. Phys. Commun. 88 (1995) 341.
[51] Y.-P. Liu, G.C. Lynch, T.N. Troung, D.-H. Lu, D.G. Truhlar, B.C. Garrett, J. Am. Chem. Soc. 115 (1993) 2408.
[52] Y. Kawashima, K. Kawaguchi, E. Hirota, J. Chem. Phys. 87 (1987) 6331.
[53] P. Brint, B. Sangchakr, P.W. Fowler, J. Chem. Soc., Faraday Trans. II 85 (1989) 29.
[54] M.L. McKee, J. Phys. Chem. 96 (1992) 5380.
[55] C.A. Thompson, L. Andrews, J.M.L. Martin, J. El-Yazal, J. Phys. Chem. 99 (1995) 13839.
[56] G.W.C. Kaye, T.H. Laby, Tables of Physical and Chemical Constants, Longman Group Limited, London, 1995.
[57] N.L. Ira, Molecular spectroscopy, Wiley, New York, 1975.